Bystander Killing of Malignant Glioma by Bone Marrow–derived Tumor-Infiltrating Progenitor Cells Expressing a Suicide Gene

Hrvoje Miletic[1],*, Yvonne Fischer[2],*, Sara Litwak[3], Tsanan Giroglou[2], Yannic Waerzeggers[4], Alexandra Winkeler[4], Huongfeng Li[4], Uwe Himmelreich[5], Claudia Lange[6], Werner Stenzel[1], Martina Deckert[1], Harald Neumann[3], Andreas H Jacobs[4],* and Dorothee von Laer[2],*

[1]Abteilung für Neuropathologie, Universität zu Köln, Köln, Germany; [2]Georg-Speyer-Haus, Frankfurt am Main, Germany; [3]Neural Regeneration Unit, Institute of Reconstructive Neurobiology, University Bonn LIFE & BRAIN Center and Hertie Foundation, Bonn, Germany; [4]Labor für Gentherapie und Molekulares Imaging, Max-Planck-Institut für Neurologische Forschung, Universität zu Köln, Köln, Germany; [5]In-vivo NMR Laboratory, Max-Planck-Institute for Neurological Research with Klaus-Joachim-Zülch-Laboratories of the Max Planck Society and the Faculty of Medicine of the University of Cologne, Köln, Germany; [6]Bone Marrow Transplant Center, University Hospital Hamburg-Eppendorf, Hamburg, Germany

Adult stem cells are promising cellular vehicles for therapy of malignant gliomas as they have the ability to migrate into these tumors and even track infiltrating tumor cells. However, their clinical use is limited by a low passaging capacity that impedes large-scale production. In the present study, a bone marrow–derived, highly proliferative subpopulation of mesenchymal stem cells (MSCs)—here termed bone marrow–derived tumor-infiltrating cells (BM-TICs)—was genetically modified for the treatment of malignant glioma. Upon injection into the tumor or the vicinity of the tumor, BM-TICs infiltrated solid parts as well as the border of rat 9L glioma. After intra-tumoral injection, BM-TICs expressing the thymidine kinase of herpes simplex virus (HSV-tk) and enhanced green fluorescent protein (BM-TIC-tk-GFP) were detected by non-invasive positron emission tomography (PET) using the tracer 9-[4-[^{18}F]fluoro-3-hydroxymethyl)butyl]guanine ([^{18}F]FHBG). A therapeutic effect was demonstrated *in vitro* and *in vivo* by BM-TICs expressing HSV-tk through bystander-mediated glioma cell killing. Therapeutic efficacy was monitored by PET as well as by magnetic resonance imaging (MRI) and strongly correlated with histological analysis. In conclusion, BM-TICs expressing a suicide gene were highly effective in the treatment of malignant glioma in a rat model and therefore hold great potential for the therapy of malignant brain tumors in humans.

INTRODUCTION

Malignant gliomas still have a dismal prognosis despite advances in neurosurgery and adjuvant radio- and chemotherapy. One major reason is their infiltrative growth pattern, with single tumor cells migrating distantly from the solid tumor mass and infiltrating normal brain tissue, where they can cause recurrent tumors. Novel therapies should aim to target these infiltrating cells, too.

One very promising therapeutic approach is the intra-tumoral delivery of adult stem cells that express therapeutic genes. Stem cells are suitable cellular vehicles for glioma therapy as they have the ability to migrate to a pathologic focus. Several groups of researchers have shown that neural and mesenchymal stem cells (NSCs and MSCs) migrate specifically to and into malignant gliomas and even track infiltrating tumor cells.[1–3] However, there are two important limitations in terms of large-scale production of these cells for clinical application. NSCs can be isolated only from fetal or adult brain or generated from embryonic stem cells. In addition, they have a very limited passaging capacity *in vitro*. MSCs, although easy accessible from the bone marrow, also have a low passaging capacity, with a maximum of up to 5–50 population doublings (PDs) *in vitro*.[4,5] So far, these stem cells can be expanded efficiently only after introduction of a growth-promoting gene. Examples are MSCs that are transfected with the human telomerase reverse transcriptase gene[4] or the murine NSC line C17.2,[6] genetically modified to express c-*myc*.

An attractive option for clinical use is a highly proliferative subpopulation of bone marrow–derived MSCs called bone marrow–derived multipotent adult progenitor cells (MAPCs), which can be expanded for more than 100 PDs without exogenous immortalization. MAPCs are pluripotent and differentiate into most somatic tissues *in vivo* when injected into an early blastocyst.[7] In our study, we derived bone marrow cells according to the original protocol published by Jiang *et al*.[7] As described for MAPCs, the isolated cells were negative for CD44, CD90, and major histocompatibility complex (MHC) class I antigens,[7] whereas all three markers are found on MSCs.[8,9] Our study focused on the tumor-infiltrating ability of this MAPC-like cell population rather than on their capacity to differentiate

* These authors contributed equally to this work.
Correspondence: Hrvoje Miletic, Abteilung für Neuropathologie, Universität zu Köln, Joseph-Stelzmann-Strasse 9, D-50931 Köln, Germany. E-mail: h.miletic@uni-koeln.de

into different lineages. Therefore, we here name these MAPC-like cells bone marrow–derived tumor-infiltrating cells (BM-TICs). BM-TICs were compared with various cell lines that can be expanded to high cell numbers for their migratory behavior in malignant glioma *in vivo*. We demonstrated that BM-TICs have

Table 1 Phenotypic characterization of rBM-TIC and rMSC

Surface markers[a]	BM-TIC	MSC
CD31	–	–
CD44	–	+
CD45	–	–
CD90	–	+
CD105	–	–
CD106	–	–
MHCI	–	+

Abbreviations: BM-TIC, bone marrow–derived tumor-infiltrating cell; MSC, mesenchymal stem cell; MHCI, major histocompatibility complex class I.
[a]Cell-surface expression of the indicated proteins was determined by flow cytometry.
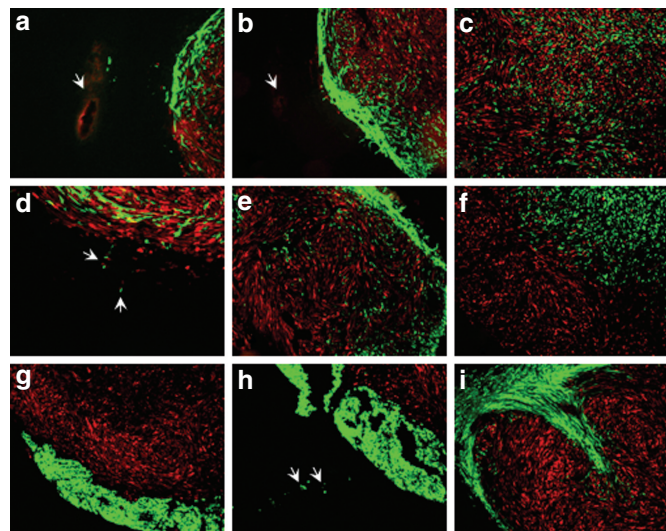

Figure 1 Migration of bone marrow–derived tumor-infiltrating cells (BM-TICs) in DsRed-transduced 9L glioma. Distinct cell lines transduced with enhanced green fluorescent protein (eGFP) were tested for migration in established 9LDsRed glioma. Cell lines were injected into or in the vicinity of glioma 5 days after tumor implantation. Histological sections were analyzed by fluorescence microscopy 3 and 7 days after implantation of cell lines. Overlays of green (eGFP cell line signal) and red (DsRed glioma signal) fluorescence are shown. (**a**) BM-TICs localized within the tumor. Individual cells were detected between the injection site (arrow) and the tumor border after 3 days. (**b**) BM-TICs migrated from the injection site (arrow) to the tumor border and into the solid tumor parts. (**c**) Distribution of BM-TICs in the tumor after 7 days. (**d**) BM-TICs (green) appeared to track tumor cells (red) infiltrating the normal tissue (arrows) 7 days after injection. (**e**) C17.2 neural stem cells showed a similar migration from border to solid tumor parts at 3 days after implantation. (**f**) 3T3 cells stayed sharply demarcated from the tumor at 3 days after injection. (**g**) K562 cells were detected at the tumor/normal brain border and did not migrate into the tumor. Jurkat and Raji cells showed a similar migration pattern (data not shown). (**h**) Few K562 cells were found in the brain parenchyma 3 days after injection. (**i**) Similar to K562 and 3T3 cells, Rat-1 cells were detected at the tumor/normal brain border and did not migrate into the tumor. (**a–c**, **e**, **f–i**) Magnification ×50. (**d**) Magnification ×100.

a migratory capacity similar to other stem cell lines, whereas hematopoietic cell lines and fibroblast control cells were unable to migrate specifically. BM-TICs were transduced with a retroviral vector expressing the thymidine kinase of herpes simplex virus (HSV-tk) and the green fluorescent protein (BM-TIC-tk-GFP) and traced by non-invasive positron emission tomography (PET). A bystander-mediated therapeutic effect of BM-TIC-tk-GFP for glioma cells was demonstrated *in vitro* and *in vivo*.

RESULTS

Phenotypic characterization of rat BM-TICs and MSCs

BM-TICs were obtained from the bone marrow of adult Fischer rats according to the protocol for isolation and expansion of MAPCs.[7] The expression of different cell-surface markers was analyzed by flow cytometry. BM-TICs were negative for CD31, CD44, CD45, CD90, CD105, CD106, and MHC class I, whereas MSCs expressed CD44, CD90, and MHC class I, as described in the literature (**Table 1**).[7–9] BM-TICs were thus phenotypically distinct from the classical MSC population.

Migratory capacity of BM-TICs and hematopoietic cell lines in 9L glioma *in vivo*

Cell lines with a high passaging capacity, which are suitable for genetic modification and large-scale production, were tested for migration in a rat glioma model. In this study, BM-TICs were used at PDs of 15–70. No major influence of the passage number on the migratory behavior described below was observed.

We investigated whether BM-TIC, K562, Jurkat, or Raji cell lines infiltrate established malignant glioma. The NSC line C17.2, for which migration has been shown in a previous study,[1] was used as positive control, and 3T3 as negative control. To rule out the interference of an immune (**Supplementary Figure S1**) response against allogeneic cell lines with their migration ability, syngeneic Fischer rat fibroblasts Rat-1 were used as a second negative control. Glioma cells (9L glioma cell line) transduced with the red fluorescence gene DsRed (9LDsRed) were implanted into the striatum of Fischer rats, and 5 days thereafter enhanced GFP (eGFP)–transduced cell lines were injected into established tumors or in the vicinity of tumors. At 3 and 7 days after implantation of the distinct cell lines, rats were killed and brain sections were analyzed by fluorescence microscopy. Within 3 days after injection, BM-TICs had migrated from the injection site to the tumor border (**Figure 1a**) as well as into the solid tumor areas (**Figure 1b**). At day 7, BM-TICs had infiltrated the majority of the solid tumor mass (**Figure 1c**) and were also found at the tumor border, even tracking tumor cells infiltrating the normal tissue (**Figure 1d**). Importantly, BM-TICs did not migrate into normal brain tissue without having been triggered by a tumor cell. The NSC line C17.2 showed a similar migratory behavior (**Figure 1e**). In contrast, 3T3 cells remained at the injection site and were well demarcated from the tumor tissue (**Figure 1f**). 3T3 cells did not migrate toward the border of the tumor or infiltrating tumor cells. The cell line K562 was detected in the brain adjacent to the tumor mass surrounding the tumor (**Figure 1g**). The same was observed for Jurkat and Raji cells (data not shown). Cells of these lines were not found in the tumor mass. However, individual cells were detected in normal
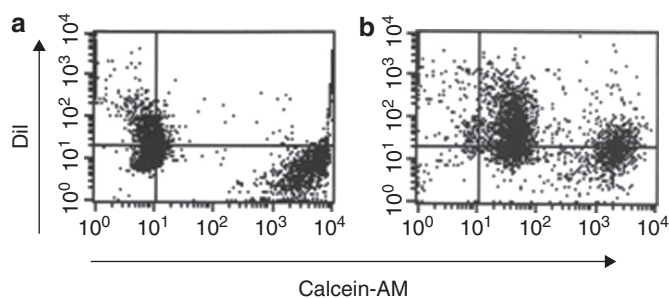
Figure 2 Gap junction formation between bone marrow–derived tumor-infiltrating cells (BM-TICs) and 9L cells. 9L cells were stained with the membrane dye DiI (red fluorescent) and BM-TICs were stained with the cytoplamic dye calcein-AM (green fluorescent), which can be transferred from cell to cell only via gap junctions. Flow cytometry measurements of dye transfer between 9L/DiI and BM-TIC/calcein-AM was assessed (**a**) immediately after mixing and (**b**) after 3 hours' incubation at 37 °C.

brain parenchyma adjacent to the tumor (**Figure 1h**). The cell line Rat-1, too, did not migrate into the tumor mass but stayed in the brain adjacent to the tumor mass (**Figure 1i**).

Gap junction formation between BM-TICs and 9L cells

The formation of gap junctions between therapeutic cells and tumor cells is critical in a suicide gene therapy approach, as gap junctions are responsible for the bystander effect. Gap junction communication between cells can be measured by dye-transfer experiments and flow cytometry.[10] In these experiments, one cell population contains a non-membrane-permeable dye that is taken up by another cell population upon incubation. Here, 9L cells were labeled with the membrane dye 1,1′-dioctadecyl-3,3,3′,3′-tetramethylindocarbocyanine perchlorate (DiI) and incubated together with BM-TICs containing the non-membrane-permeable dye calcein-AM. As shown in **Figure 2a**, 9L/DiI and BM-TIC/calcein-AM cells form two distinct populations of either red- or green-fluorescent cells immediately after mixing. After 3 hours of incubation, however, 9L/DiI cells have taken up green-fluorescent calcein-AM and appear as a population of double-positive red- and green-fluorescent cells (**Figure 2b**), whereas BM-TICs have lost intensity of green fluorescence owing to transfer of calcein-AM and taken up more DiI. DiI cannot be transferred from one cell to another as it is a membrane-bound protein. However, DiI can be set free from apoptotic cells (during the incubation period, by trypsinization, before or during flow cytometry) and thereafter can bind to the membrane of living cells (9L cells and BM-TICs), which might explain the shift in both populations. In contrast, cytoplasmatic or free calcein-AM can be taken up by a living cell only via gap junctions. Therefore, the shift of 9L/DiI in the direction of calcein-AM can be explained only by gap-junctional communication.

In vitro bystander killing of 9L glioma cells by BM-TICs expressing HSV-tk

BM-TICs were transduced with a retroviral vector expressing the HSV-tk suicide gene (BM-TIC-tk; see Materials and Methods). The bystander killing effect of BM-TIC-tk on 9L-DsRed glioma cells was examined by co-culture experiments. After addition of
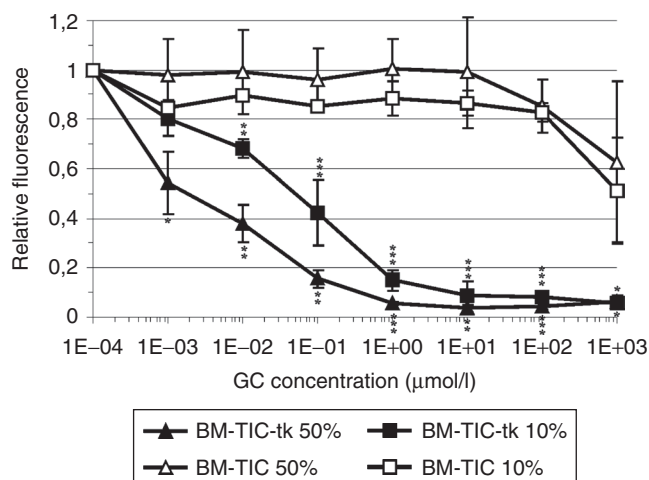

Figure 3 Bystander effect of bone marrow–derived tumor-infiltrating cells expressing the thymidine kinase (BM-TIC-tk) on 9L glioma cells *in vitro*. Mixed cultures of 9L-DsRed cells containing either 50 or 10% BM-TIC or BM-TIC-tk, respectively, were incubated with ganciclovir (GC) at increasing concentrations. After 3 days, cells were lysed and the fluorescence intensity of DsRed in the lysates, corresponding to the number of living 9L glioma cells, was quantified with an automated 96-well plate fluorescence reader. The graph shows mean fluorescence and standard deviations from three independent experiments. *P* refers to levels of statistical significance between BM-TIC 50% and BM-TIC-tk 50% (indicated above single values) and BM-TIC 10% and BM-TIC-tk 10% (indicated underneath single values). Student's *t*-test for non-discrete grade values. $^*P < 0.05$, $^{**}P < 0.01$, $^{***}P < 0.001$.

ganciclovir (GC) to the medium, BM-TIC-tk exerted a strong and dose-dependent bystander effect on glioma cells (**Figure 3**). Killing of 90% of glioma cells was achieved in cultures containing 50% or even only 10% BM-TIC-tk. Killing was statistically significant with GC concentrations ranging from 10^{-3} to 10^3 μmol/l for 50% BM-TIC-tk and from 10^{-2} to 10^3 μmol/l for 10% BM-TIC-tk. In contrast, 9LDsRed cells mixed with native BM-TICs were resistant to GC up to high concentrations (**Figure 3**). These experiments show that BM-TIC-tk can be used to deliver toxic molecules, such as phosphorylated GC, to glioma cells.

In vivo bystander killing of 9L glioma cells by BM-TIC-tk-GFP

To analyze the therapeutic effect of BM-TICs *in vivo*, BM-TICs transduced with HSV-tk and GFP (BM-TIC-tk-GFP) were injected into 9L tumors 5 days after tumor implantation. As a control, non-migrating Rat-1 transduced with HSV-tk and GFP (Rat-1-tk-GFP) were implanted. From day 4 after cell injection, one group of BM-TIC-implanted rats ($n = 9$), one group of Rat-1-implanted rats ($n = 8$), and one control group implanted with 9L only ($n = 8$) received daily intraperitoneal injections of 30 mg per kg GC for 10 days. Two control groups of BM-TIC-tk-GFP- ($n = 8$) or Rat-1-tk-GFP-implanted rats ($n = 8$) were not treated with GC. Kaplan–Meier survival analysis showed more than 60% long-term survivors in the BM-TIC-tk-GFP plus GC–treated group surviving for 110 days (**Figure 4a**). Two out of nine animals died at day 28, and one died at day 54 after tumor implantation. All animals in the control groups died within the observation period. Thus, treated animals showed a prolonged survival compared with both
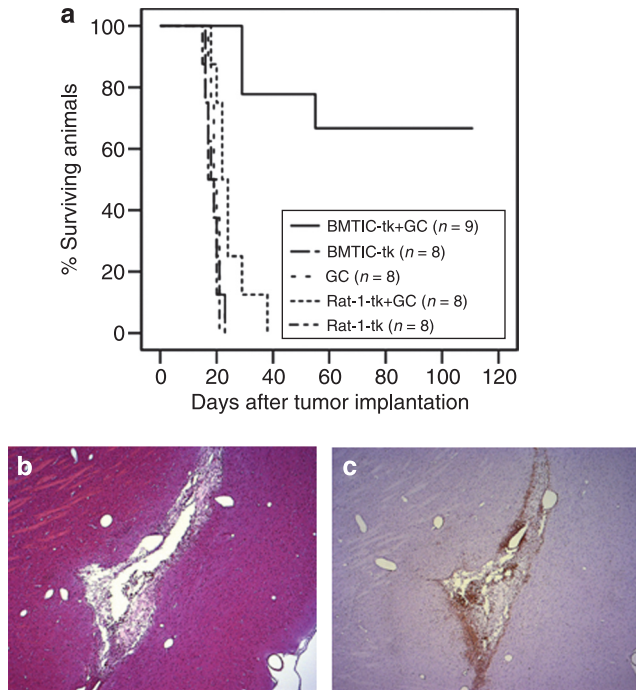
Figure 4 Bystander effect of bone marrow–derived tumor-infiltrating cells (BM-TICs) expressing the thymidine kinase (BM-TIC-tk) and green fluorescent protein (BM-TIC-tk-GFP) on 9L glioma *in vivo*. BM-TIC-tk-GFP or Rat-1-tk-GFP cells were injected into 9L tumors (groups BM-TIC-tk-GFP, BM-TIC-tk-GFP + ganciclovir (GC), Rat-1-tk-GFP, and Rat-1-tk-GFP + GC) 5 days after tumor cell implantation in adult rats. One group (GC) received 9L cells only. Four days after BM-TIC-tk-GFP or Rat-1-tk-GFP implantation, the groups GC, BM-TIC-tk-GFP + GC, and Rat-1-tk-GFP + GC were treated with GC for 10 days. (**a**) In total 66.67% of rats survived 110 days in the BM-TIC-tk-GFP plus GC–treated group. The graph shows the Kaplan–Meier survival curve. The difference in survival between the treated group and control groups was statistically significant ($P < 0.001$; log-rank test). The Rat-1-tk-GFP + GC–treated group survived significantly shorter compared with the BM-TIC-tk-GFP + GC–treated group ($P < 0.01$; log rank test). (**b**) Histological analysis of brains of long-term survivors in the BM-TIC-tk-GFP + GC–treated group revealed a cavity and scar formation at the initial site without tumor cells. Hematoxylin and eosin staining, original magnification ×25. (**c**) CD45^{+} leukocytes infiltrate the scar tissue. Anti-CD45-staining, original magnification ×25.

control groups that was statistically highly significant ($P < 0.001$). In contrast, Rat-1-tk-GFP and GC–treated animals showed a significantly reduced survival compared with BM-TIC-tk-GFP and GC–treated animals ($P < 0.01$), but also a significantly prolonged survival compared with control groups ($P < 0.05$).

Tumor cells were not detected on serial histological sections in the brains of BM-TIC-tk-GFP plus GC–treated long-term survivors. A cavity and scar tissue resulting from the initial tumor mass, which had been successfully treated, was observed in long-term survivors and was infiltrated by CD45-positive inflammatory cells (**Figure 4b** and **c**).

Detection of HSV-1-tk-GFP-transduced BM-TICs and therapeutic follow-up by PET and MRI

For clinical application of therapeutic cells, it is essential to be able to locate these cells using non-invasive methods. For this purpose, BM-TIC-tk-GFP cells were injected into 9LDsRed tumors, and
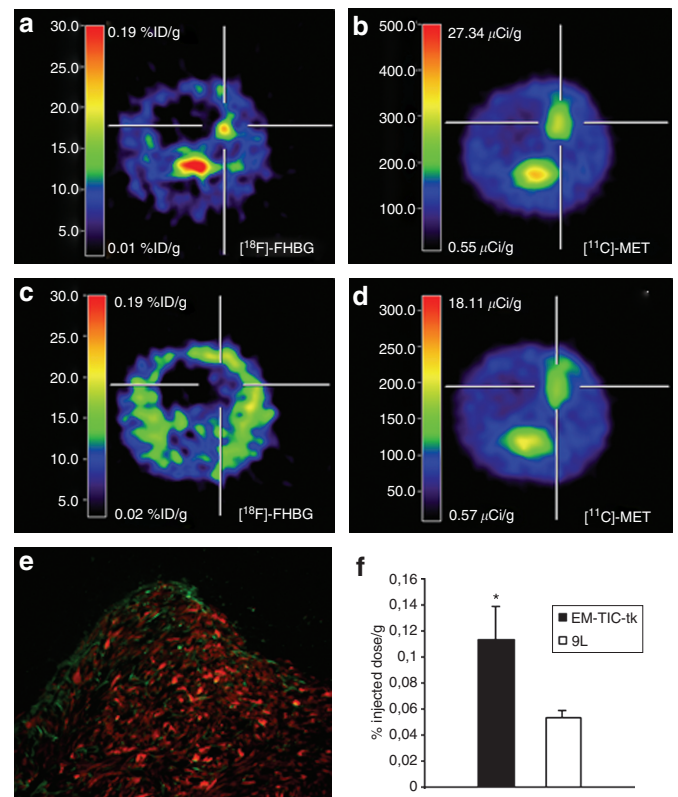

Figure 5 Detection of bone marrow–derived tumor-infiltrating cells (BM-TICs) expressing the thymidine kinase and green fluorescent protein (BM-TIC-tk-GFP) by positron emission tomography (PET) imaging. BM-TIC-tk-GFP cells were injected into 9LDsRed tumors, and 6–7 days later 9-[4-[^{18}F]fluoro-3-hydroxymethyl)butyl]guanine ([^{18}F]FHBG) PET scans were performed. In addition, methyl-[^{11}C]-l-methionine [^{11}C]MET PET scans and magnetic resonance imaging (MRI) scans for detection of the 9LDsRed tumor were performed on different days. On day 7 after BM-TIC-tk-GFP implantation, animals were perfused and fluorescence microscopy was applied for detection of BM-TIC-tk-GFP. (**a**) [^{18}F]FHBG PET scan of a BM-TIC-tk-injected animal showing HSV-tk expression in the tumor area with a maximum of 0.14% of injected dose/g. (**b**) [^{11}C]MET PET scan of the same animal detecting 9LDsRed tumor 7 days after tumor implantation. (**c**) [^{18}F]FHBG PET scan of a control animal (9LDsRed only) showing low [^{18}F]FHBG uptake in the tumor area with a maximum of 0.05% of injected dose/g. (**d**) [^{11}C]MET PET scan of the same animal detecting 9LDsRed tumor 7 days after tumor implantation. (**e**) Enhanced GFP (eGFP)–positive BM-TIC-tk-GFP cells are detected at the tumor border and the solid tumor part. Overlay of green (BM-TIC-tk-GFP) and red (9LDsRed tumor) fluorescence. Magnification ×50. (**f**) Histogram showing relative HSV-tk expression level. [^{18}F]FHBG uptake in BM-TIC-tk-GFP-injected animals (0.113 ± 0.025% of the injected dose/g; $n = 3$) was significantly higher ($P < 0.05$) than in the control group (0.053 ± 0.006% of injected dose/g; $n = 3$). Shown are the mean values of each group. P refers to levels of statistical significance between the BM-TIC-tk-GFP and 9LDsRed-only groups. Student's t-test for non-discrete grade values. *$P < 0.05$.

9-[4-[^{18}F]fluoro-3-hydroxymethyl)butyl]guanine ([^{18}F]FHBG) PET scans for detection of BM-TIC-tk-GFP were applied 6–7 days later. [^{18}F]FHBG is the specific substrate for HSV-tk and therefore confirms HSV-tk expression *in vivo*. In addition, methyl-[^{11}C]-l-methionine ([^{11}C]MET) PET scans and magnetic resonance imaging (MRI) scans for detection of the 9LDsRed tumor were performed up to 22 days. BM-TIC-tk-GFP cells were detected in the tumor (**Figure 5a** and **b**), and fluorescence microscopy of
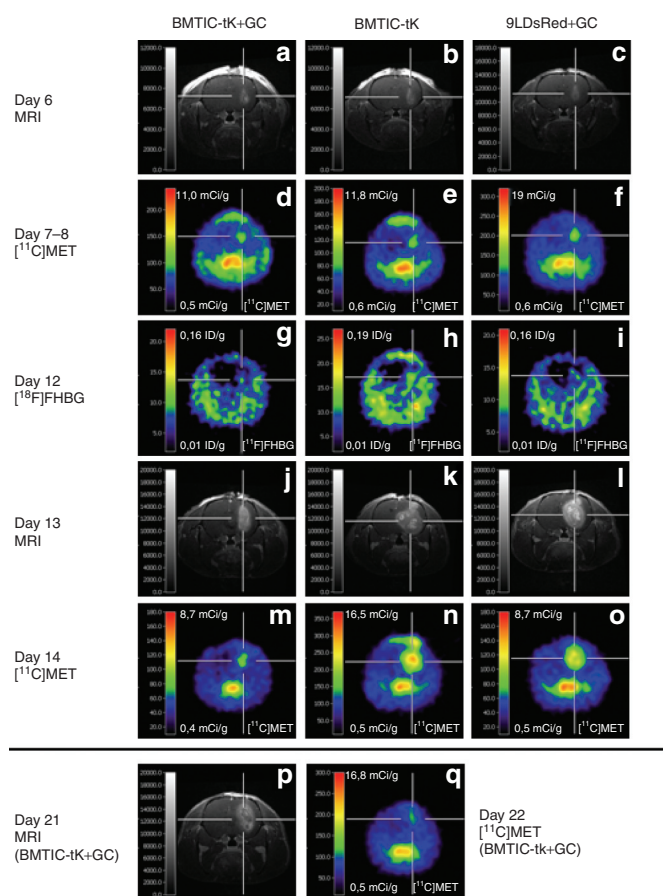
Figure 6 Magnetic resonance imaging (MRI) and positron emission tomography (PET) imaging for therapeutic follow-up. Representative three-dimensional MRI (T1-weightened FLASH, echo time = 5 ms, repetition time = 70 ms, 60° pulse, resolution 121 × 121 × 242 μm, post-administration of gadopentetic acid (Gd-DTPA), [^{18}C] methyl-[^{18}C]-L-methionine MET PET and [^{18}F] 9-[4-[^{18}F]fluoro-3-hydroxymethyl)butyl]guanine FHBG PET scans. Time points after tumor implantation: (**a–c**) 6 days, MRI before ganciclovir (GC) treatment; (**d–f**) 7–8 days, [^{18}C]MET PET before GC treatment; (**g–i**) 12 days, [^{18}F]FHBG PET during GC treatment; (**j–l**) 13 days, MRI during GC treatment; (**m–o**) 14 days, [^{18}C]MET PET during GC treatment; (**p**) 21 days, MRI after GC treatment; (**q**) 22 days [^{18}C]MET PET after GC treatment. The three different groups were treated as described for the survival study: (**a, d, g, j, m, p, q**) bone marrow–derived tumor-infiltrating cells expressing the thymidine kinase of green fluorescent protein (BM-TIC-tk-GFP) injection with GC treatment; (**b, e, h, k, n**) BM-TIC-tk-GFP injection without GC treatment; (**c, f, i, l, o**) 9LDsRed only with GC treatment.

histological sections confirmed eGFP-positive cells at the border and in solid tumor parts (**Figure 5e**). The relative expression level of HSV-tk was 0.113 ± 0.025% of the injected dose/g tissue (**Figure 5f**). In contrast, animals that had received glioma cells only (control group) had a significantly lower [^{18}F]FHBG uptake in the tumor (0.053 ± 0.006% of injected dose/g; $P < 0.05$; **Figure 5c–d** and **f**).

For treatment with GC, the animals were divided into three groups as described above for the survival study. On day 6 and day 7 or 8 after tumor implantation and before GC treatment, tumors were detected by MRI and [^{18}C]MET PET scans, respectively (**Figure 6a–f**). In animals without GC treatment, implanted

BM-TIC-tk-GFP cells were detected by [^{18}F]FHBG PET scans 7 days after implantation (**Figure 6h**). In contrast, animals with 3 days of GC treatment had an uptake similar to control animals that received 9LDsRed cells and GC (**Figure 6g** and **i**), indicating loss of HSV-tk activity as a result of the treatment. Five days after initiation of GC treatment, the tumor size of treated animals was reduced compared with both control groups, as shown on MRI and [^{18}C]MET PET scans (**Figure 6j–o**). As determined by semiquantitative estimations based on the size of the hyperintense lesion in gadopentetic acid–enhanced (Gd-DTPA) three-dimensional MRI, the tumor size in the treated animals was 20–40% that of both controls on day 13. Three to five days after termination of GC application, animals with a good response to treatment exhibited a low contrast-enhancing lesion in MRI (**Figure 6p**) and only a very weak signal in [^{18}C]MET PET (**Figure 6q**). The hyperintense lesion for individual animals increased from day 7–8 to day 13 by a factor of 1.7 ± 0.3 for the treated animals and by a factor of 6.1 ± 0.5 for both control groups. The lesion size in the treated animals did not change significantly between day 13 (during GC treatment) and day 21 (after GC treatment; change by a factor of 0.95 ± 0.1). Compared with day 13, lesion appearance in the final MRIs was very heterogeneous, indicating the possible presence of cystic and necrotic compartments. By histology, only residual tumor cells were detected, surrounded and intermingled with CD45-positive inflammatory cells (**Figure 7a, d** and **e**). The latter consisted predominantly of CD8$^+$ T cells. In addition, CD4$^+$ T cells, ED1$^+$ macrophages, and CD161$^+$ natural killer cells were seen (**Figure 7f–i**). In both control groups, animals became terminally ill during the treatment and were killed. Histology revealed large tumor masses (**Figure 7b** and **c**) that contained less prominent leukocytic infiltrations compared with the treated group (**Figure 7j–o**).

These data demonstrate that PET imaging is a suitable method to detect therapeutic cells *in vivo*. Furthermore, the strong correlation with histological data confirmed that PET/MRI is a useful method to monitor the therapeutic response non-invasively in individual animals.

DISCUSSION

This study demonstrates that a subpopulation of bone marrow–derived MSCs can be used as tumor-infiltrating therapeutic cells against malignant glioma. These BM-TICs exhibited a migratory behavior similar to that of NSCs and MSCs.[1–3] They migrated from the injection site to the border of the tumor and also infiltrated solid tumor parts. Importantly, they even appeared to track infiltrating glioma cells, as already described for NSCs by Aboody et al.[1] This feature is of great significance because, at present, infiltrating glioma cells cannot be targeted successfully and are therefore responsible for recurrent tumors and the poor prognosis of glioblastoma patients.

However, the use of NSCs and MSCs in clinical application is hampered by their low passaging capacity, which is in the range 5–50 PDs.[4,5] A higher passaging capacity can be obtained only by gene modification of stem cells with oncogenes or other genes promoting cell proliferation.[4,6] But these modifications are associated with a higher risk of tumorigenicity. In this regard, it has been demonstrated that long-term cultures of telomerase-transduced
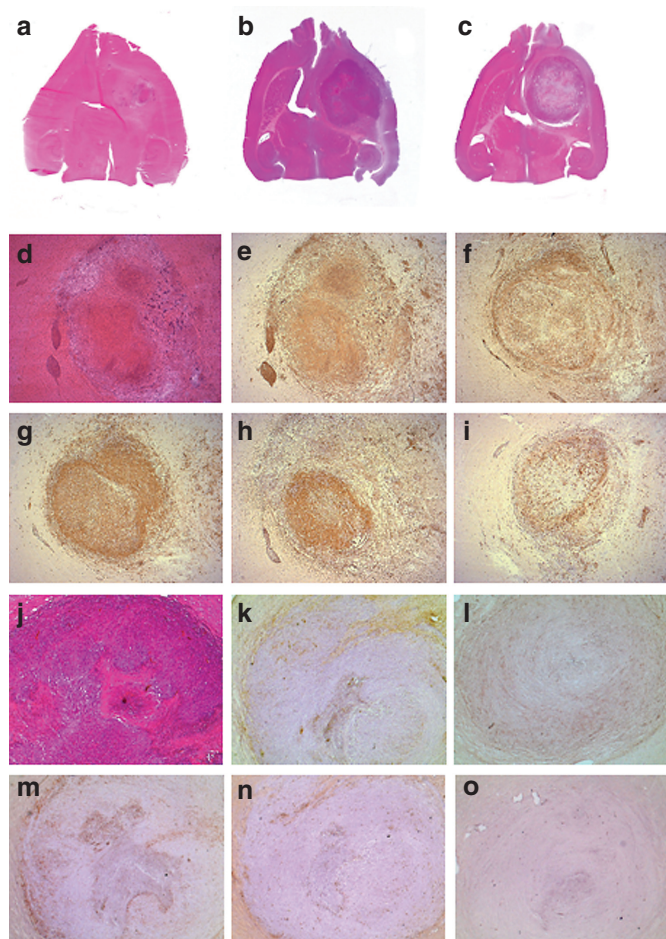
Figure 7 Histology and immunohistochemistry. Animals were killed and perfused when they became terminally ill or, in the therapeutic group, 4–8 days after end of ganciclovir (GC) treatment. (**a–c**) Macroscopic photographs of transversal brain sections. Hematoxylin and eosin (H&E) staining. (**a**) Bone marrow–derived tumor-infiltrating cells (BM-TICs) expressing the thymidine kinase and green fluorescent protein (BM-TIC-tk-GFP) injected and GC–treated animal with a small lesion. Control animals show large tumor masses. (**b**) BM-TIC-injected animal. (**c**) Control animal with 9LDsred only and GC treatment. (**d–i**) Animal shown in **a** at higher magnification (×25) and immunohistochemistry. (**d**) Residual tumor cells infiltrated by inflammatory cells. H&E staining. (**e**) Inflammatory cells are identified as CD45+ leukocytes, which consist of (**f**) CD4+ T cells, (**g**) CD8+ T cells, (**h**) ED1+ macrophages and microglia, and (**i**) CD161+ natural killer cells. (**j–o**) Control animal shown in **b** at higher magnification (×25) and immunohistochemistry. (**j**) Large tumor mass with necrotic areas and no obvious immune cell infiltration. H&E staining. (**k**) CD45+ leukocytes are detected around necrotic areas and at the tumor border and are less prominent compared with the therapeutic group. Leukocytes consist of (**l**) CD4+ T cells, (**m**) CD8+ T cells, (**n**) ED1+ macrophages and microglia, and (**o**) few CD161+ NK cells. Original magnification ×25.

human MSCs may accumulate spontaneous genetic changes leading to tumorigenicity in immunodeficient mice.[11] A second obstacle for clinical application is that NSCs can be isolated only from fetal or adult brain or from embryonic stem cells. In contrast, the BM-TICs used in this study have all the requirements for an applicable glioma therapy: they can be isolated easily from bone marrow, they can be passaged for more than 100 PDs,[7] and they show a specific migration in malignant glioma.

Phenotypically, BM-TICs were found to resemble the MAPCs described by Verfaillie's group and to differ substantially from classical MSC: rat BM-TICs stained negative for CD44, CD90, and MHC class I, as first reported by Jiang et al. for MAPCs,[7] whereas rat MSCs express these markers. CD44, CD90, and MHC class I are also expressed on human MSCs[8,9,12] but are absent or expressed at low levels (CD44) on human MAPCs.[13]

Furthermore, we demonstrated that gene-modified BM-TICs can be used for glioma therapy in rats. Our cell culture experiments showed that BM-TIC-tk-GFP cells exert a strong bystander effect on 9L glioma cells upon GC treatment. *In vivo*, more than 60% of BM-TIC-tk-GFP plus GC–treated animals were long-term survivors. In contrast, animals treated with non-migrating, syngeneic fibroblasts Rat-1-tk-GFP plus GC survived significantly shorter, without long-term survival. The HSV-tk/GC system is considered to be highly effective for cancer therapy.[14–17] The prodrug GC is phosphorylated by the enzyme HSV-tk into cytotoxic GC-P and is transported via gap junctions to neighboring cells, thus exerting a bystander effect on non-gene-modified cells.[18] The role of gap junctions in this process has been verified by co-culture experiments of connexin-expressing and connexin-deficient cells.[19] We confirmed gap junction communication between BM-TICs and 9L cells by dye transfer of calcein-AM. Calcein-AM is non-fluorescent until it is taken up by cells and cleaved by cellular esterases. Processed calcein-AM is a green fluorescent dye that does not diffuse through the cellular membrane. However, intercellular transfer of calcein-AM can occur through cell–cell communication channels (gap junctions), which can be measured by flow cytometry.[10] This communication is the basis for the strong therapeutic bystander effect of the HSV-tk/GC system, which can compensate for low transduction efficiencies. Thus, the HSV-tk/GC system is widely used in strategies targeting various types of cancer cells by viral vectors. However, clinical trials for glioma using this system have failed.[20,21] One major reason may be the delivery method of HSV-tk into glioma cells: viral vectors and fibroblasts used as packaging cells for viral vectors both mediate gene modification of cells only in the direct vicinity of the injection site and therefore fail to transduce infiltrating tumor cells or distant tumor areas. In this study, migrating BM-TICs modified with a therapeutic gene that exerts a bystander effect could partially overcome this problem.

An even greater therapeutic efficacy might be achieved if the infiltrating cells were modified to produce a viral vector that transfers the therapeutic gene(s) efficiently and selectively to the tumor cells. NSCs expressing HSV-tk have been shown to mediate a therapeutic bystander effect *in vitro* and *in vivo* similar to that observed in our study.[22,23] However, the establishment of a stable packaging cell line for *in vivo* delivery of viral vectors based on NSCs would be hampered by the low expansion capacity of these cells. In this regard, our recently established stable packaging cell line based on BM-TICs producing retroviral vectors pseudotyped with glycoproteins of the lymphocytic choriomeningitis virus, a vector pseudotype that transduces glioma cells with a high specificity and efficacy,[24–27] may be useful. In fact, upon injection into 9L rat glioma, packaging cells showed a similar intra-tumoral distribution to that reported here and mediated transduction of glioma cells in solid as well as infiltrating tumor parts.[28]

In addition to its therapeutic effect, HSV-tk has gained increasing attention as a marker for non-invasive imaging. The expression of the HSV-tk protein, which selectively incorporates certain radiolabeled nucleoside analogues into DNA,[29–31] can be non-invasively imaged in distinct regions of a transduced tissue.[29,32–37] Therefore, HSV-tk-based PET imaging has been used to evaluate the transduction efficiency of viral vector–mediated gene therapy applications *in vivo*.[38–40] In our study, this technique was applied to localize therapeutic cells *in vivo*. The visualization of therapeutic cells within a tumor is an important clinical issue as the intra-tumoral distribution of these cells is the prerequisite for an efficient therapeutic effect. Using the HSV-tk-specific tracer [18F]FHBG, BM-TIC-tk-GFP cells were detected intra-tumorally *in vivo* by PET imaging 6–7 days after implantation. The uptake of [18F]FHBG in BM-TIC-tk-GFP-injected animals was significantly (twofold) increased compared with the control group. The intra-tumoral localization of BM-TIC-tk-GFP cells was confirmed by fluorescence microscopy of histological sections. Furthermore, BM-TIC-tk-GFP-injected and GC-treated animals showed a lower [18F]FHBG uptake in the tumor area than BM-TIC-tk-GFP-injected and non-GC-treated animals, indicating loss of HSV-tk activity as a result of the treatment. In fact, to our knowledge, this is the first demonstration that therapeutic cells can be non-invasively imaged intra-cerebrally by PET. Although Shah *et al.* detected intra-cerebrally migrating NSCs by bioluminescence imaging of glioma in nude mice,[41] this technique has not been established for clinical use. In contrast, the feasibility of [124I]FIAU PET imaging for detection of HSV-tk-transduced tumor cells in patients with malignant glioma has already been demonstrated.[42]

In addition, the therapeutic effect of BM-TIC-tk-GFP treatment was monitored successfully during and after termination of GC treatment by MRI and [11C]MET PET imaging. In general, tumors of animals in the therapeutic group were reduced in size compared with those of control animals. Histopathology revealed only residual tumor cells in the treatment group and large tumor masses in both control groups, showing that imaging data were strongly correlated with histology. Furthermore, a strong immune reaction was evident at the initial tumor site of treated animals, predominantly consisting of CD8^{+} T cells with additional CD4^{+} T cells, ED1^{+} macrophages, and CD161^{+} natural killer cells, whereas control animals showed less prominent leukocytic infiltrates in large tumor masses. These data suggest that the therapeutic effect was in part mediated by the immune response. A similar immunologic bystander effect was observed in other gene therapy studies using viral vectors or viral vector packaging cell lines to deliver HSV-tk to tumor cells.[14,43]

In conclusion, in bone marrow–derived progenitor cells, all relevant features for the translation of a cell-based therapy into the clinic are combined. In addition to their migratory ability, they show a high passaging capacity, which allows genetic modification and large-scale production. Furthermore, they can be non-invasively imaged *in vivo* and they transmit a bystander-mediated and immune response–supported therapeutic effect through the HSV-tk/GC paradigm in experimental malignant glioma.

MATERIALS AND METHODS

Cell lines. The human embryonic kidney cell line 293T [American Type Culture Collection (ATCC) number CRL-11268], the murine fibroblast cell line NIH 3T3 (ATCC number CRL-1658), the 9L cell line, and the syngeneic Fischer rat fibroblast cell line Rat-1 were obtained from ATCC (Manassas, VA) and maintained in Dulbecco's modified Eagle's medium supplemented with 10% fetal calf serum and 1% glutamine. The B-cell line Raji (ATCC number CRL-86), the T-cell line Jurkat (ATCC number TIB-152), and the myeloid cell line K562 (ATCC number CCL-243) were obtained from ATCC and maintained in Roswell Park Memorial Institute 1640 medium supplemented with 10% fetal calf serum and 1% glutamine. All cell lines were grown in a humidified atmosphere of 5% CO_2.

Isolation and culture of rat MSCs. MSCs were isolated from rats and cultured as previously described.[44]

BM-TIC isolation and culture. BM-TICs were prepared from bone marrow as previously described.[7]

Flow cytometry. Surface expression of cells was analyzed by flow cytometry on a FACSCalibur (Becton Dickinson, San Jose, CA). Rat-specific antibodies against CD44 (clone Ox-49), CD45 (clone Ox-1), CD90 (clone Ox-7), MHC class I (clone Ox-18), CD31 (clone TLD-3A12), and CD106 (clone MR106) were purchased from BD Pharmingen (Heidelberg, Germany). Anti-CD105 (sc-19793) antibody was obtained from Santa Cruz (Heidelberg, Germany).

Vector construction. A retroviral vector containing the *hsv-tk39* gene, an internal ribosome entry site (IRES) region, and a puromycin resistance gene and a second retroviral vector containing the *hsv-tk39* gene, an IRES region, and a *gfp* gene were constructed. For further information, see **Supplementary Materials and Methods**.

Preparation of retroviral vector supernatants. The 293T cell line was used for transient vector production as described in detail previously.[24]

Retroviral marking of cell lines with the eGFP. To express the marker protein eGFP stably, cells were transduced with the retroviral vector MP71-eGFP-wPRE. For further information see **Supplementary Materials and Methods**.

Transduction of BM-TICs and Rat-1 cells with the hsv-tk39 gene. BM-TICs were transduced with the retroviral vector MP91-TK-IRES-Puro or MP91-TK-IRES-GFP, which co-expressed a *hsv-tk39* gene and a puromycin resistance gene or *hsv-tk39* gene and a GFP gene, respectively. Rat-1 cells were transduced with MP91-TK-IRES-GFP. For further information see **Supplementary Materials and Methods**.

Transduction of 9L cells with DsRed. 9L cells were transduced as described previously.[25]

Double-dye transfer assay. To assess gap junction communication between 9L glioma cells and BM-TICs, 9L cells were stained with the membrane-binding red fluorescent dye DiI (Molecular Probes, Karlsruhe, Germany), whereas BM-TICs were stained with calcein-AM (Molecular Probes). Stainings with DiI (5 µl per ml cell suspension) and calcein-AM (0.75 µM) were performed according to the manufacturer's instructions. After staining, 9L cells and BM-TICs were washed three times with phosphate-buffered saline, mixed at a ratio of 1:1, and seeded at 5×10^5 cells/well into 24-well plates. Cells were incubated for 3 hours at 37 °C. Calcein-AM transfer from BM-TICs to 9L cells was assessed using a flow cytometer (BD, Heidelberg, Germany).

Bystander-mediated killing of 9L cells in vitro. Mixtures of 9LDsRed with BM-TIC-tk cells or 9LDsRed with BM-TICs were seeded into fibronectin-coated 96-well plates in Dulbecco's modified Eagle's medium supplemented with 5% fetal calf serum. Mixtures contained either 10% or 50% BM-TIC-tk cells or BM-TICs, respectively. The total cell number per well was 1×10^4 cells. Cells were incubated for 4 hours; thereafter, medium was

changed and 100 μl Dulbecco's modified Eagle's medium supplemented with 5% fetal calf serum containing increasing concentrations of GC was added. After a 3-day incubation period, medium was removed, and cells were washed three times with phosphate-buffered saline and subsequently lysed by adding 100 μl of radio-immunoprecipitation assay buffer [150 mmol/l NaCl, 50 mmol/l Tris, 1% (vol/vol) Triton X-100, pH 7.3]. Fluorescence intensity in the lysates, corresponding to the number of living 9LDsRed cells at the time of cell lysis, was determined using a Fluorostar Optima plate reader (BMG Labtechnologies, Offenburg, Germany).

Implantation of 9L and cell lines. Adult female Fisher 344 rats (Harlan Winkelmann, Borchen, Germany) were anesthetized by intra-peritoneal injection of ketamine (50 mg per kg) and xylazine (2 mg per kg). Intracranial 9LDsRed or 9L tumors were established by injection of 8×10^4 9LDsRed cells or 6×10^4 9L cells (in 2 μl phosphate-buffered saline) into the right striatum, respectively, using a Hamilton syringe in a stereotactic apparatus (Stoelting, Wood Dale, IL). The coordinates used were 4 mm lateral to the bregma and 5 mm below the dural surface. Five days after tumor implantation, rats were anesthetized, and different cell lines were injected using the same stereotactic coordinates. In the migration experiment 10^5 cells and in the treatment experiments 6×10^5 cells of each cell line were implanted.

Analysis of migration of test cells within brain tumors. Animals were killed and perfused with 4% paraformaldehyde. Brains were removed, suspended in 30% sucrose for 3 days, and snap-frozen in isopentane chilled with liquid nitrogen. Coronal cryostat sections (12 μm) were prepared and examined under a fluorescence microscope (Zeiss, Jena, Germany). All animal procedures were carried out in accordance with the regulations established by the German Committee for Animal Care and Use.

Treatment of rat gliomas. Fischer rats either bearing 9L tumors or bearing 9L tumors and having been implanted with BM-TIC-tk-GFP or Rat-1-tk-GFP were treated by daily intraperitoneal injections of 30 mg per kg GC for 10 days, starting at day 4 after BM-TIC-tk-GFP or Rat-1-tk-GFP implantation.

Histology and immunohistochemistry. Animals were killed and perfused as described above. Cryostat sections were stained with hematoxylin and eosin (H&E; Merck, Darmstadt, Germany). For immunohistochemistry, the primary mouse anti-rat antibodies directed against LCA (Becton Dickinson, Heidelberg, Germany), CD4 (Becton Dickinson), CD8 (Becton Dickinson), ED1 (Acris, Hiddenhausen, Germany), and CD161 (Becton Dickinson) were used. Immunohistochemistry was performed using the avidin–biotin-complex technique with appropriate biotinylated secondary antibodies (Vectastain Elite kit; Vector Laboratories, Burlingame, CA) and visualizing peroxidase reaction product using 3,3′-diaminobenzidine (Sigma, Munich, Germany) as chromogene and H_2O_2 as co-substrate.

Radiosynthesis of radiotracers [¹¹C]Methionin and [¹⁸F]FHBG. The radiotracer for tumor detection, [¹¹C]MET, and the specific radiolabeled marker substrate for HSV-tk, [¹⁸F]FHBG, were produced as described previously.[39,45]

PET. PET imaging was performed using a microPET (Concorde Microsystems, Knoxville, TN; 63 image planes; 2.0 mm full width at half maximum). Radiotracer was administered intravenously (caudal vein) into experimental animals at the following doses: no-carrier-added [¹¹C]MET: 670–1111 μCi/rat; no-carrier-added [¹⁸F]FHBG: 390–480 μCi/rat. Emission scans (duration 30 minutes) were obtained starting 10 minutes ([¹¹C]MET) and more than 120 minutes ([¹⁸F]FHBG) after tracer application. Images were reconstructed using Fourier rebinning and two-dimensional filtered-back projection (microPET). For quantification of images, a reference standard sample of radiotracer was placed within the field of view of the PET scanner. Image registration and data

evaluation based on a region-of-interest (ROI) analysis of PET images to determine maximal radioactivity concentrations within tumors were performed using VINCI (MPI Cologne, Cologne, Germany), a newly developed, fast graphical image analysis tool.[46] After background (contralateral hemisphere) subtraction, data were decay-corrected and divided by the total injected dose to represent percentage injected dose per gram.

Localization of tumor before and during gene therapy was performed by MRI and [¹¹C]MET PET. The respective PET images were registered to the MRIs.

MRI. Animals were imaged after administration of approximately 1 ml/g body weight gadopentetic acid (500 mM, Magnevist; Schering, Berlin, Germany). Animals were anesthetized using 1% halothane in $O_2:N_2O$ (35:65%). Temperature was maintained at 37 °C and monitored throughout the MRI measurements. All MRIs were acquired using a Bruker Biospin 4.7 T small-animal scanner (Ettlingen, Germany; horizontal bore, 30 cm) equipped with actively shielded gradients (200 mT/m). Purpose-built radio-frequency coils were used (12-cm Helmholtz coils for excitation and a 3-cm surface coil for detection). After two-dimensional localization scans, three-dimensional gradient-echo scans (FLASH) with T1 weighting were acquired. The acquisition parameters were spatial resolution = $121 \times 121 \times 242$ μm³, field of view = $31 \times 31 \times 15.5$ mm³, repetition time = 70 ms, echo time = 5 ms, flip angle = 60°. Images were processed using Paravision 3.2 (Bruker Biospin, Karlsruhe, Germany) and VINCI for registration with PET data. Lesion volumes were estimated based on the hyperintense region in three-dimensional T1-weighted images after gadopentetic acid administration using the National Institutes of Health program ImageJ.

Statistical analysis. Survival was analyzed with a log-rank test based on the Kaplan–Meier test using SPSS software (SPSS GmbH, Munich, Germany). Differences between pairs of groups were determined using the Student's *t*-test. $P < 0.05$ was considered significant.

SUPPLEMENTARY MATERIAL
Figure S1. Leukocytic infiltrations of 9LDsRed tumors injected with different cell lines.
Materials and Methods.

REFERENCES
1. Aboody, KS, Brown, A, Rainov, NG, Bower, KA, Liu, S, Yang, W *et al.* (2000). Neural stem cells display extensive tropism for pathology in adult brain: evidence from intracranial gliomas. *Proc Natl Acad Sci USA* **97**: 12846–12851.

2. Nakamizo, A, Marini, F, Amano, T, Khan, A, Studeny, M, Gumin, J *et al.* (2005). Human bone marrow-derived mesenchymal stem cells in the treatment of gliomas. *Cancer Res* **65**: 3307–3318.

3. Nakamura, K, Ito, Y, Kawano, Y, Kurozumi, K, Kobune, M, Tsuda, H *et al.* (2004). Antitumor effect of genetically engineered mesenchymal stem cells in a rat glioma model. *Gene Ther* **11**: 1155–1164.

4. Hamada, H, Kobune, M, Nakamura, K, Kawano, Y, Kato, K, Honmou, O *et al.* (2005). Mesenchymal stem cells (MSC) as therapeutic cytoreagents for gene therapy. *Cancer Sci* **96**: 149–156.

5. Colleoni, S, Donofrio, G, Lagutina, I, Duchi, R, Galli, C and Lazzari, G (2005). Establishment, differentiation, electroporation, viral transduction, and nuclear transfer of bovine and porcine mesenchymal stem cells. *Cloning Stem Cells* **7**: 154–166.

6. Snyder, EY, Deitcher, DL, Walsh, C, Arnold-Aldea, S, Hartwieg, EA and Cepko, CL (1992). Multipotent neural cell lines can engraft and participate in development of mouse cerebellum. *Cell* **68**: 33–51.

7. Jiang, Y, Jahagirdar, BN, Reinhardt, RL, Schwartz, RE, Keene, CD, Ortiz-Gonzalez, XR *et al.* (2002). Pluripotency of mesenchymal stem cells derived from adult marrow. *Nature* **418**: 41–49.

8. Mareschi, K, Ferrero, I, Rustichelli, D, Aschero, S, Gammaitoni, L, Aglietta, M *et al.* (2006). Expansion of mesenchymal stem cells isolated from pediatric and adult donor bone marrow. *J Cell Biochem* **97**: 744–754.

9. Stute, N, Holtz, K, Bubenheim, M, Lange, C, Blake, F and Zander, AR (2004). Autologous serum for isolation and expansion of human mesenchymal stem cells for clinical use. *Exp Hematol* **32**: 1212–1225.

10. Czyz, J, Irmer, U, Schulz, G, Mindermann, A and Hulser, DF (2000). Gap-junctional coupling measured by flow cytometry. *Exp Cell Res* **255**: 40–46.

11. Serakinci, N, Guldberg, P, Burns, JS, Abdallah, B, Schrodder, H, Jensen, T *et al.* (2004). Adult human mesenchymal stem cell as a target for neoplastic transformation. *Oncogene* **23**: 5095–5098.

12. Shur, I, Marom, R, Lokiec, F, Socher, R and Benayahu, D (2002). Identification of cultured progenitor cells from human marrow stroma. *J Cell Biochem* **87**: 51–57.

13. Reyes, M, Lund, T, Lenvik, T, Aguiar, D, Koodie, L and Verfaillie, CM (2001). Purification and *ex vivo* expansion of postnatal human marrow mesodermal progenitor cells. *Blood* **98**: 2615–2625.

14. Barba, D, Hardin, J, Sadelain, M and Gage, FH (1994). Development of anti-tumor immunity following thymidine kinase-mediated killing of experimental brain tumors. *Proc Natl Acad Sci USA* **91**: 4348–4352.

15. Chen, SH, Shine, HD, Goodman, JC, Grossman, RG and Woo, SL (1994). Gene therapy for brain tumors: regression of experimental gliomas by adenovirus-mediated gene transfer *in vivo. Proc Natl Acad Sci USA* **91**: 3054–3057.

16. Moolten, FL and Wells, JM (1990). Curability of tumors bearing herpes thymidine kinase genes transferred by retroviral vectors. *J Natl Cancer Inst* **82**: 297–300.

17. Moolten, FL, Wells, JM, Heyman, RA and Evans, RM (1990). Lymphoma regression induced by ganciclovir in mice bearing a herpes thymidine kinase transgene. *Hum Gene Ther* **1**: 125–134.

18. Culver, KW, Ram, Z, Wallbridge, S, Ishii, H, Oldfield, EH and Blaese, RM (1992). *In vivo* gene transfer with retroviral vector-producer cells for treatment of experimental brain tumors. *Science* **256**: 1550–1552.

19. Mesnil, M, Piccoli, C, Tiraby, G, Willecke, K and Yamasaki, H (1996). Bystander killing of cancer cells by herpes simplex virus thymidine kinase gene is mediated by connexins. *Proc Natl Acad Sci USA* **93**: 1831–1835.

20. Rainov, NG (2000). A phase III clinical evaluation of herpes simplex virus type 1 thymidine kinase and ganciclovir gene therapy as an adjuvant to surgical resection and radiation in adults with previously untreated glioblastoma multiforme. *Hum Gene Ther* **11**: 2389–2401.

21. Sandmair, AM, Loimas, S, Puranen, P, Immonen, A, Kossila, M, Puranen, M *et al.* (2000). Thymidine kinase gene therapy for human malignant glioma, using replication-deficient retroviruses or adenoviruses. *Hum Gene Ther* **11**: 2197–2205.

22. Li, S, Tokuyama, T, Yamamoto, J, Koide, M, Yokota, N and Namba, H (2005). Bystander effect-mediated gene therapy of gliomas using genetically engineered neural stem cells. *Cancer Gene Ther* **12**: 600–607.

23. Uhl, M, Weiler, M, Wick, W, Jacobs, AH, Weller, M and Herrlinger, U (2005). Migratory neural stem cells for improved thymidine kinase-based gene therapy of malignant gliomas. *Biochem Biophys Res Commun* **328**: 125–129.

24. Beyer, WR, Westphal, M, Ostertag, W and von Laer, D (2002). Oncoretrovirus and lentivirus vectors pseudotyped with lymphocytic choriomeningitis virus glycoprotein: generation, concentration, and broad host range. *J Virol* **76**: 1488–1495.

25. Miletic, H, Fischer, YH, Neumann, H, Hans, V, Stenzel, W, Giroglou, T *et al.* (2004). Selective transduction of malignant glioma by lentiviral vectors pseudotyped with lymphocytic choriomeningitis virus glycoproteins. *Hum Gene Ther* **15**: 1091–1100.

26. Beyer, WR, Miletic, H, Ostertag, W and von Laer, D (2001). Recombinant expression of lymphocytic choriomeningitis virus strain WE glycoproteins: a single amino acid makes the difference. *J Virol* **75**: 1061–1064.

27. Miletic, H, Bruns, M, Tsiakas, K, Vogt, B, Rezai, R, Baum, C *et al.* (1999). Retroviral vectors pseudotyped with lymphocytic choriomeningitis virus. *J Virol* **73**: 6114–6116.

28. Fischer, H, Miletic, H, Giroglov, T, Litwak, S, Stenzel, W, Deckert, M *et al.* (2007). A retroviral packaging cell line for LCMV pseudotype vectors based on tumor-infiltrating progenitor cells. *J Gene Med* (in press).

29. Gambhir, SS, Barrio, JR, Wu, L, Iyer, M, Namavari, M, Satyamurthy, N *et al.* (1998). Imaging of adenoviral-directed herpes simplex virus type 1 thymidine kinase reporter gene expression in mice with radiolabeled ganciclovir. *J Nucl Med* **39**: 2003–2011.

30. Saito, Y, Price, RW, Rottenberg, DA, Fox, JJ, Su, TL, Watanabe, KA *et al.* (1982). Quantitative autoradiographic mapping of herpes simplex virus encephalitis with a radiolabeled antiviral drug. *Science* **217**: 1151–1153.

31. Tjuvajev, JG, Stockhammer, G, Desai, R, Uehara, H, Watanabe, K, Gansbacher, B *et al.* (1995). Imaging the expression of transfected genes *in vivo. Cancer Res* **55**: 6126–6132.

32. Gambhir, SS, Barrio, JR, Phelps, ME, Iyer, M, Namavari, M, Satyamurthy, N *et al.* (1999). Imaging adenoviral-directed reporter gene expression in living animals with positron emission tomography. *Proc Natl Acad Sci USA* **96**: 2333–2338.

33. Gambhir, SS, Herschman, HR, Cherry, SR, Barrio, JR, Satyamurthy, N, Toyokuni, T *et al.* (2000). Imaging transgene expression with radionuclide imaging technologies. *Neoplasia* **2**: 118–138.

34. Hospers, GA, Calogero, A, van Waarde, A, Doze, P, Vaalburg, W, Mulder, NH *et al.* (2000). Monitoring of herpes simplex virus thymidine kinase enzyme activity using positron emission tomography. *Cancer Res* **60**: 1488–1491.

35. Tjuvajev, JG, Finn, R, Watanabe, K, Joshi, R, Oku, T, Kennedy, J *et al.* (1996). Noninvasive imaging of herpes virus thymidine kinase gene transfer and expression: a potential method for monitoring clinical gene therapy. *Cancer Res* **56**: 4087–4095.

36. Tjuvajev, JG, Avril, N, Oku, T, Sasajima, T, Miyagawa, T, Joshi, R *et al.* (1998). Imaging herpes virus thymidine kinase gene transfer and expression by positron emission tomography. *Cancer Res* **58**: 4333–4341.

37. Tjuvajev, JG, Chen, SH, Joshi, A, Joshi, R, Guo, ZS, Balatoni, J *et al.* (1999). Imaging adenoviral-mediated herpes virus thymidine kinase gene transfer and expression *in vivo. Cancer Res* **59**: 5186–5193.

38. Yaghoubi, SS, Barrio, JR, Namavari, M, Satyamurthy, N, Phelps, ME, Herschman, HR *et al.* (2005). Imaging progress of herpes simplex virus type 1 thymidine kinase suicide gene therapy in living subjects with positron emission tomography. *Cancer Gene Ther* **12**: 329–339.

39. Jacobs, AH, Winkeler, A, Hartung, M, Slack, M, Dittmar, C, Kummer, C *et al.* (2003). Improved herpes simplex virus type 1 amplicon vectors for proportional coexpression of positron emission tomography marker and therapeutic genes. *Hum Gene Ther* **14**: 277–297.

40. Penuelas, I, Mazzolini, G, Boan, JF, Sangro, B, Marti-Climent, J, Ruiz, M *et al.* (2005). Positron emission tomography imaging of adenoviral-mediated transgene expression in liver cancer patients. *Gastroenterology* **128**: 1787–1795.

41. Shah, K, Bureau, E, Kim, DE, Yang, K, Tang, Y, Weissleder, R *et al.* (2005). Glioma therapy and real-time imaging of neural precursor cell migration and tumor regression. *Ann Neurol* **57**: 34–41.

42. Voges, J, Reszka, R, Gossmann, A, Dittmar, C, Richter, R, Garlip, G *et al.* (2003). Imaging-guided convection-enhanced delivery and gene therapy of glioblastoma. *Ann Neurol* **54**: 479–487.

43. Rainov, NG, Kramm, CM, Aboody-Guterman, K, Chase, M, Ueki, K, Louis, DN *et al.* (1996). Retrovirus-mediated gene therapy of experimental brain neoplasms using the herpes simplex virus-thymidine kinase/ganciclovir paradigm. *Cancer Gene Ther* **3**: 99–106.

44. Lange, C, Bassler, P, Lioznov, MV, Bruns, H, Kluth, D, Zander, AR *et al.* (2005). Liver-specific gene expression in mesenchymal stem cells is induced by liver cells. *World J Gastroenterol* **11**: 4497–4504.

45. Berger, G, Maziere, M, Knipper, R, Prenant, C and Comar, D (1979). Automated synthesis of 11C-labelled radiopharmaceuticals: imipramine, chlorpromazine, nicotine and methionine. *Int J Appl Radiat Isot* **30**: 393–399.

46. Cizek, J, Herholz, K, Vollmar, S, Schrader, R, Klein, J and Heiss, WD (2004). Fast and robust registration of PET and MR images of human brain. *Neuroimage* **22**: 434–442.